

Proton-transfer based azides with fluorescence off–on response for detection of hydrogen sulfide. An experimental, theoretical and bioimaging study

Claudia B da Silva, Eduarda S Gil, Fabiano da Silveira Santos, Ana M Moras, Luiza Steffens, Paulo F. B. Goncalves, Dinara J Moura, Diogo S. Lüdtke, and Fabiano Severo Rodembusch

J. Org. Chem., **Just Accepted Manuscript** • DOI: 10.1021/acs.joc.8b02489 • Publication Date (Web): 26 Nov 2018

Downloaded from <http://pubs.acs.org> on November 27, 2018

Just Accepted

“Just Accepted” manuscripts have been peer-reviewed and accepted for publication. They are posted online prior to technical editing, formatting for publication and author proofing. The American Chemical Society provides “Just Accepted” as a service to the research community to expedite the dissemination of scientific material as soon as possible after acceptance. “Just Accepted” manuscripts appear in full in PDF format accompanied by an HTML abstract. “Just Accepted” manuscripts have been fully peer reviewed, but should not be considered the official version of record. They are citable by the Digital Object Identifier (DOI®). “Just Accepted” is an optional service offered to authors. Therefore, the “Just Accepted” Web site may not include all articles that will be published in the journal. After a manuscript is technically edited and formatted, it will be removed from the “Just Accepted” Web site and published as an ASAP article. Note that technical editing may introduce minor changes to the manuscript text and/or graphics which could affect content, and all legal disclaimers and ethical guidelines that apply to the journal pertain. ACS cannot be held responsible for errors or consequences arising from the use of information contained in these “Just Accepted” manuscripts.

Proton-transfer based azides with fluorescence off–on response for detection of hydrogen sulfide. An experimental, theoretical and bioimaging study

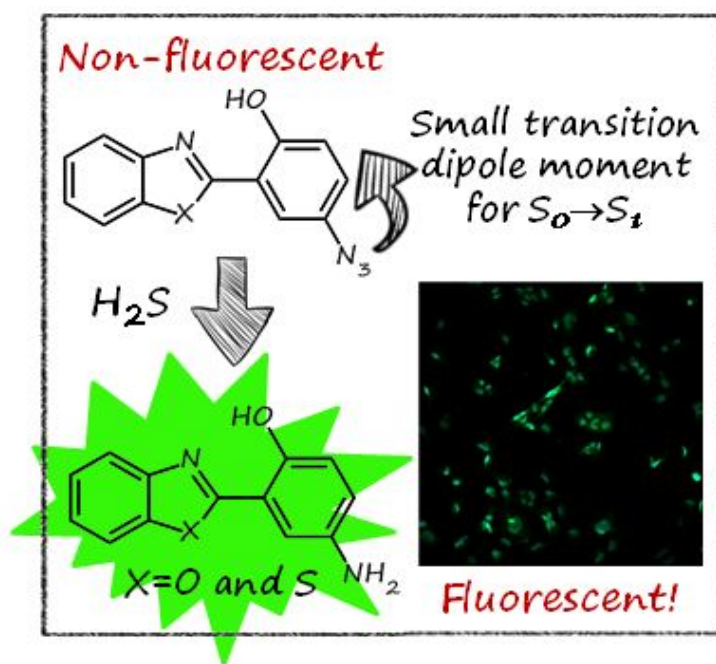
Cláudia Brito da Silva,^a Eduarda Sangiogo Gil,^a Fabiano da Silveira Santos,^a Ana Moira Morás,^b Luiza Steffens,^b Paulo Fernando Bruno Gonçalves,^a Dinara Jaqueline Moura,^b Diogo Seibert Lüdtkke,^a Fabiano Severo Rodembusch^{*,a}

^aInstituto de Química, Universidade Federal do Rio Grande do Sul, UFRGS. Av. Bento Gonçalves 9500, 91501-970, Porto Alegre, RS, Brazil. Phone: +55 51 3308 9637.

E-mail: rodembusch@iq.ufrgs.br

^bLaboratório de Genética Toxicológica, Universidade Federal de Ciências da Saúde de Porto Alegre, Rua Sarmento Leite, 245, 90050-170, Porto Alegre, Rio Grande do Sul, Brazil

Graphical Abstract:



Abstract. This work describes the synthesis of photoactive proton transfer compounds based on the benzazolic core containing the azide group. The compounds present absorption in the UV region and fluorescence emission in the visible region of the spectra with large Stokes shift due to a phototautomerism in the excited state (ESIPT). The azide location on the benzazolic structure showed to present a noteworthy role on their photophysics leading to fluorescence quenching. A photophysical study was performed in the presence of NaHS to evaluate their application as H₂S sensor. The methodology employed was the reduction of azides to amines using NaHS to mimic H₂S, resulting in an off–on response fluorescence mechanism. The observed photophysical features were successfully used to explore the azides as fluorescent probes in biological media. In addition, DFT and TD-DFT calculations with CAM-B3LYP/cc-pVDZ and CAM-B3LYP/jun-cc-pVTZ level respectively were performed in order to understand the photophysics features of azide derivatives, where the main interest was investigate fluorescence quenching experimentally observed in the azide derivatives.

Keywords: ESIPT, optical sensor, azides, TD-DFT, fluorescence

Introduction

Hydrogen sulfide (H₂S) is a small and colorless gas molecule that has a characteristic odor, which may cause irritation to eyes and respiratory system under prolonged exposure.^{1,2} H₂S is produced primarily through the decomposition of organic compounds or as by-products of industries such as oil refining, agriculture, mining, manufacturing of organophosphorus pesticides, etc.^{3,4} Although hydrogen sulfide exhibits chronic and acute toxicity in high concentrations, causing a variety of disease phenotypes such as Alzheimer's disease, hypertension, liver cirrhosis, Down syndrome and diabetes,⁵⁻⁸ in low concentrations H₂S can positively influence physiological effects, including regulation of blood pressure, oxygen sensor, neuromodulation, mitochondrial energy production and anti-inflammatory action.⁹⁻¹⁸

Several methods of hydrogen sulfide evaluation have been developed,¹⁹ including electrochemical analysis,^{20,21} gas chromatography,^{21,22} and colorimetric and or fluorometric methods.²³⁻²⁶ Among these methods the emission of fluorescence is considered one of the most efficient methods due to sensitivity and simplicity and biological compatibility.^{27,28} In recent years fluorescent and colorimetric probes have

received considerable attention because of their unique advantages such as low cost, high throughput and naked eye detection.²⁹⁻³¹ However, the H₂S probes still have single detection window and short excitation wavelengths.³² Thus, it is required to design probes for detection of H₂S with double detection window with emission in a broad region of the electromagnetic spectrum, as observed for detection of sulfur based analytes, which present emission at the NIR region.³³⁻³⁶ In this way, a wide variety of fluorescent probes for this specific detection have been proposed in the literature (Figure 1).³⁷⁻⁴⁰ These probes follow different mechanisms, such as azide to amine or nitro to amine reductions,⁴¹⁻⁴³ R-O cleavage,^{44,45} S-O cleavage^{46,47} or double bond addition reaction.^{48,49} In this context, in this work is presented the synthesis, photophysical characterization and application of azide-containing dyes, based on the benzazole core, for the detection of H₂S in solution, using NaHS as mimic compound (Figure 1).

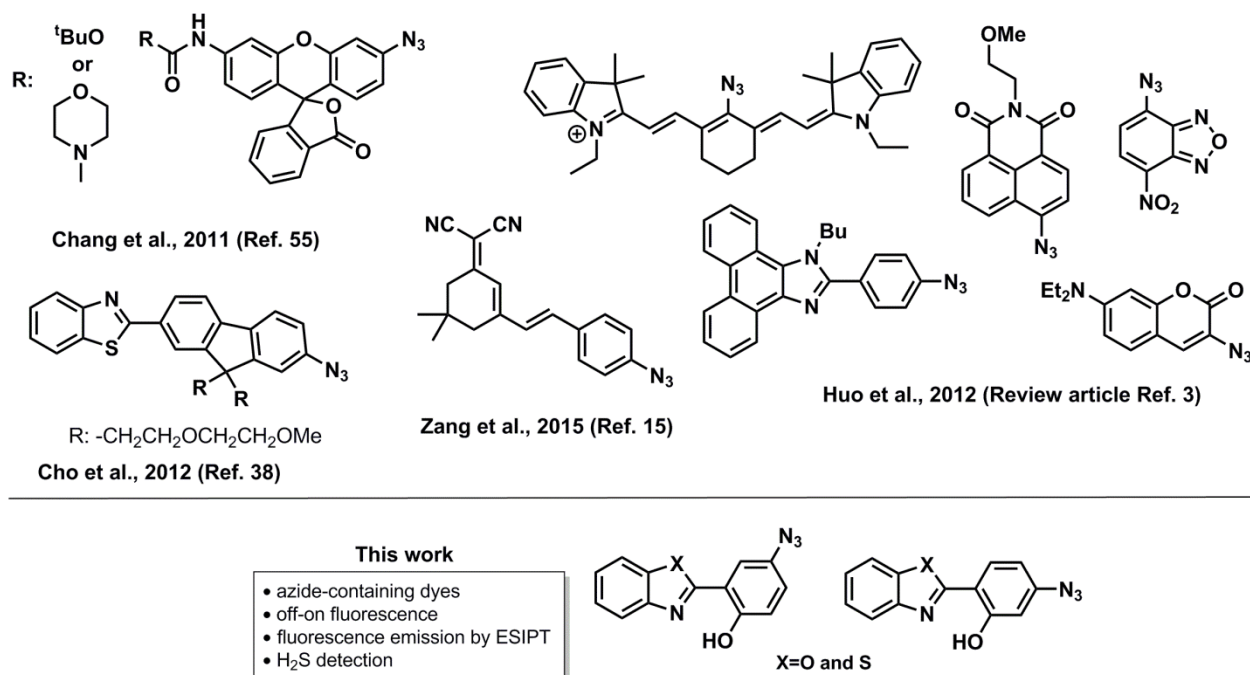
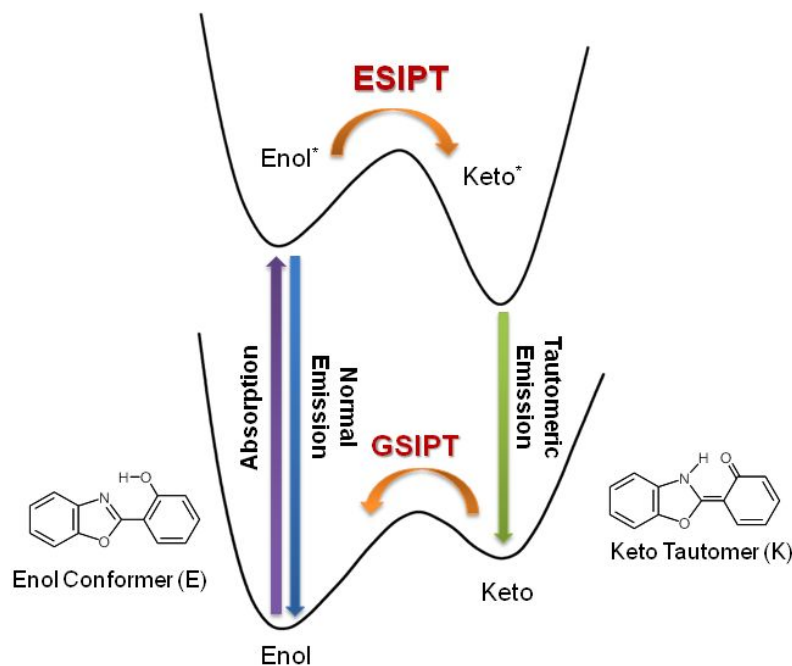


Figure 1. Examples of azide derivatives described in the literature for H₂S sensing and azide-containing dyes used in the current work.

The mechanism employed for the H₂S detection was based on the off-on fluorescence related to the reduction of azides to amines, leading to an increase in fluorescence intensity. These particular compounds present fluorescence emission since they are reactive to proton transfer in the excited state (ESIPT) (Scheme 1). In this process, after radiation absorption, a locally excited enol species (E*) that presents a proton donor, usually related to an amino or hydroxyl group, is more acidic than in the

ground state. At the same time, the acceptor group, usually imino/azonitrogen- or carbonyl-oxygen-containing ring skeleton is also more basic. These photoacidity/basicity together with distance and angle requirements, allows a faster proton transfer to produce a keto phototautomer (K^*), which decays emitting fluorescence with large Stokes shift.⁵⁰⁻⁵² In addition, in association with the observed photophysical properties, these compounds were also evaluated as fluorescent probes in cellular media.



Scheme 1. Model for the ESIPT process for a benzazole dye. The asterisk indicates the excited-state.

Results and Discussion

Photophysical characterization

The absorption spectra of the azides **6-7** and **11-12** are shown in Figure 2. The relevant data calculated from UV-Vis absorption spectroscopy for all compounds are presented in Table 1.

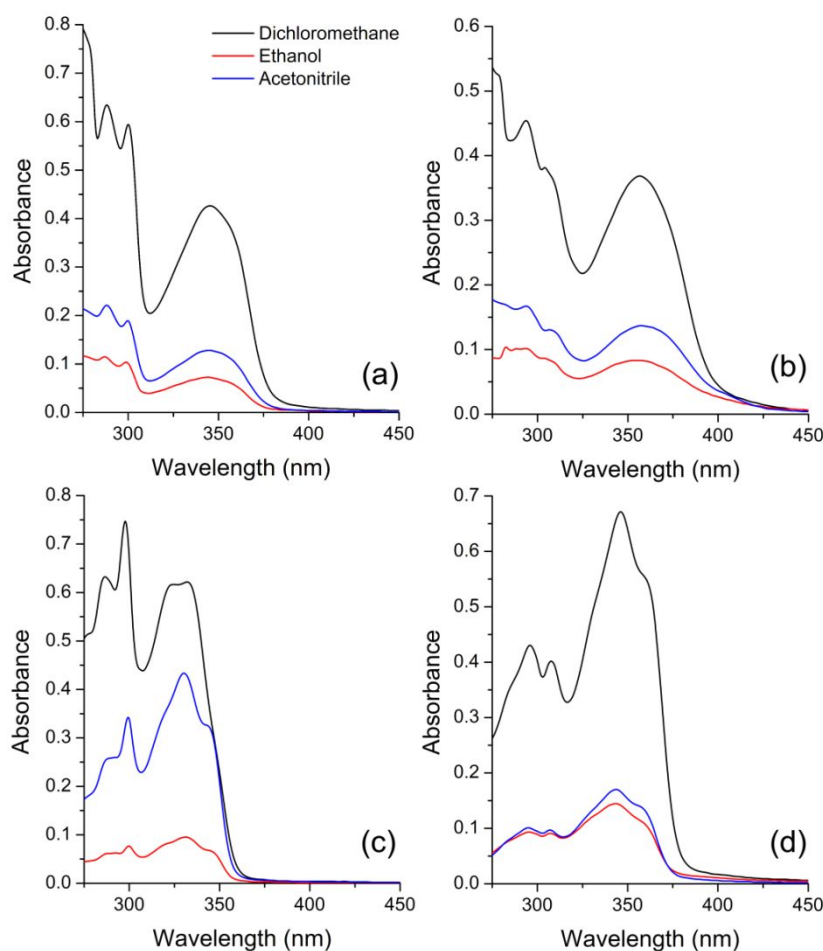


Figure 2. UV-Vis absorption spectra in solution (10^{-6} M) of the azides (a) **6**, (b) **7**, (c) **11** and (d) **12** in different organic solvents.

It can be observed an absorption maxima located in the UV region between 330-358 nm with molar absorptivity coefficient values (ϵ) related to allowed $^1\pi \rightarrow \pi^*$ electronic transitions. Despite the absorption in the UV region for all studied samples, dyes **6-7** present in general a more intense absorption band located below 300 nm, ascribed to the benzazole chromophore. This photophysical feature can be related to the difference of planarity of the dyes,^{53,54} where the less planar structures **6-7** do not allow a more effective electronic delocalization among the two π systems (phenolic and benzazolic rings), which is confirmed taking the molar extinction coefficient values in account. In addition, it could also be observed that the benzothiazole derivatives **7** and **12** presented redshifted absorption bands in despite of the benzoxazole ones (**6** and **11**), related to the better electron delocalization allowed by the sulfur atom in the benzothiazole core, as already observed in similar compounds.⁵⁴

Table 1. Photophysical data in the ground state of azides **6-7** and **11-12**, where λ_{abs} is the absorption maxima (nm) and ϵ is the molar absorptivity coefficient ($10^4 \text{ M}^{-1} \text{ cm}^{-1}$).

Azide	Solvent	λ_{abs}	ϵ
6	Dichloromethane	346	1.45
	Ethanol	345	0.24
	Acetonitrile	345	0.45
7	Dichloromethane	356	1.23
	Ethanol	358	0.28
	Acetonitrile	358	0.45
11	Dichloromethane	331	3.13
	Ethanol	330	0.47
	Acetonitrile	330	2.17
12	Dichloromethane	345	3.59
	Ethanol	343	0.77
	Acetonitrile	343	0.95

The fluorescence emission spectra of the azide derivatives **6-7** and **11-12** in solution are shown in Figure 3. The emission curves were obtained by exciting the compounds at the absorption maxima wavelengths (λ_{abs}). The data from fluorescence emission spectroscopy are also summarized in Table 2.

It can be observed that the studied azides present a photophysical behavior in the excited state that is dependent on the azide group position. The compounds **6-7** with the azide group in the 5' position are almost non fluorescent in all studied solvents. Despite the weak fluorescence intensity, a dual fluorescence emission can be observed in ethanol and dichloromethane, which confirms the conformational equilibrium in solution in the ground state.^{50,54} In these compounds, it can be observed an emission located higher than 500 nm, ascribed to the ESIPT process (Keto* emission). Additionally, a blue shifted emission, located around 400 nm was observed and related to the normal emission (Enol* emission). In acetonitrile, both derivatives show only a very weak ESIPT emission. On the other hand, derivatives presenting the azide group in the 4' position (**11-12**) present a higher fluorescence intensity with both enol (370 nm and 390 nm for X=O and S, respectively) and keto (470 nm and 500 nm for X=O and S, respectively) emission at similar location than observed to the analogues **6-7** (Figure 3).

Table 2. Photophysical data in the excited state of azides **6-7** and **11-12**, where λ_{em} is the emission maxima (nm), $\Delta\lambda_{ST}$ is the Stokes shift (nm/cm⁻¹) and Φ_{FL} ($\times 10^{-3}$) is the fluorescence quantum yield.

Azide	Solvent	λ_{em}		$\Delta\lambda_{ST}$		Φ_{FL}
		N*	K*	N*	K*	
6	Dichloromethane	382	522	36/2724	176/9745	1.1
	Ethanol	-	503	-	158/9105	4.7
	Acetonitrile	-	512	-	167/9454	1.5
7	Dichloromethane	420	537	64/4280	181/9468	11.6
	Ethanol	438	532	80/5102	174/9136	3.5
	Acetonitrile	420	551	62/4123	193/9784	2.0
11	Dichloromethane	376	473	45/3616	142/9070	58.5
	Ethanol	369	473	39/3203	143/9161	24.4
	Acetonitrile	376	474	46/3707	144/9206	11.5
12	Dichloromethane	399	500	54/3923	155/8986	7.2
	Ethanol	390	495	47/3513	152/8952	12.1
	Acetonitrile	392	504	49/3644	161/9313	10.6

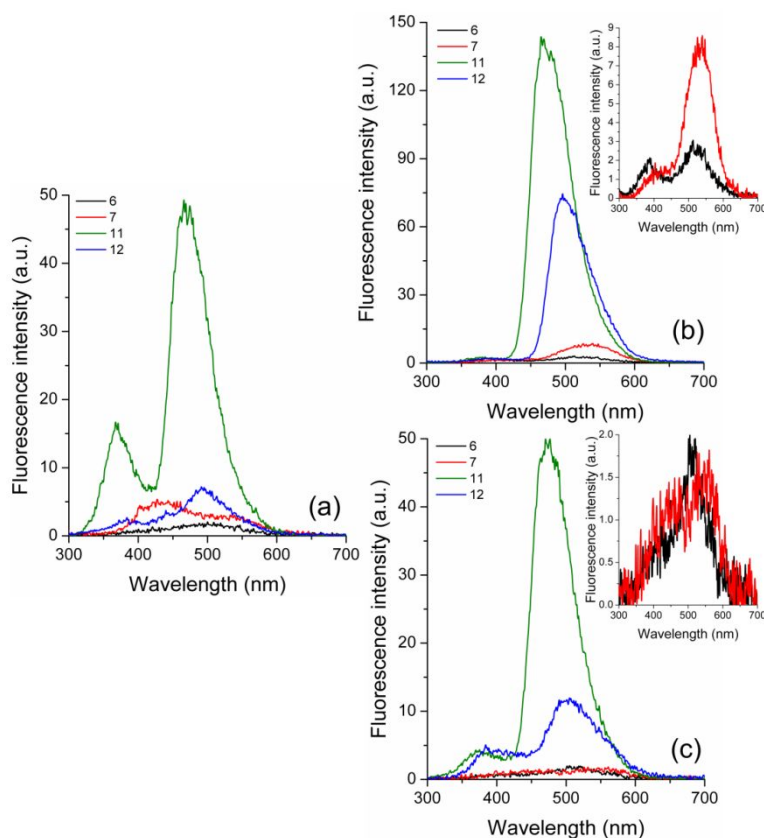


Figure 3. Steady-state fluorescence emission spectra of the azides **6-7** and **11-12** in solution (10^{-6} M) of (a) ethanol, (b) dichloromethane and (c) acetonitrile (Exc./Em. slits 5.0 nm/3.0 nm).

Once again, the benzothiazole derivatives presented redshifted bands in despite of the benzoxazole analogues, related to the better electron delocalization allowed by the sulfur atom. It is worth mentioning that it can be observed from the literature that usually azide compounds present an almost absent or very weak fluorescence emission, which can be related to a photoinduced electron transfer (PET) mechanism afforded by the $-N_3$ group.^{2,3,24,55-57} However, based on the fluorescence results presented in this work, the presence of the $-N_3$ group seems not to be enough to the expected fluorescence quenching in such derivatives. Moreover, the fluorescence quenching seems to be significantly favored when the azide group is located in the para position relative to the hydroxyl group, as shown in compounds **6-7**. In this sense, the experimental results indicate that an additional or even a different mechanism than PET is tailoring the fluorescence emission in these compounds. Additional photophysical experiments were also performed at extreme pH for comparison with the data at pH 7.4 (data not shown, see Figures S33-36).

Photophysical response of azides to NaHS

The UV-Vis absorption of the azides **6-7** and **11-12** was investigated upon addition of NaHS (1.0×10^{-3} M) in ethanol/PBS buffer solution (50/50, v/v, pH=7.4) at room temperature (Figure 4). It can be observed that significant changes took place in their absorption spectra in presence of NaHS. These compounds showed absorption peaks around 350 nm. After addition of 10 μ L NaHS, the absorption intensity of the azide increases and shifts to longer wavelengths. The observed shift on the absorption maxima of dyes **6** (~16 nm), **7** (~ 42 nm), **11** (~ 12 nm) and **12** (~ 28 nm) indicates that there was a change in the chemical structure as the result of the reduction of the azide functional group to an amino group.⁵⁴ Although the UV-Vis spectra seems to not present any clear tendency, since it changes the maxima location, as well as its intensity, it could be possible to obtain a linear correlation in the range (9.09×10^{-6} - 3.03×10^{-5} M) between the absorption with the added amount of NaHS taking the absorption maxima of the reduced compound into account (insets of Figure 4). This preliminary result using NaHS already indicates that these azides can be used as probe for the quantitative detection of H_2S in solution.

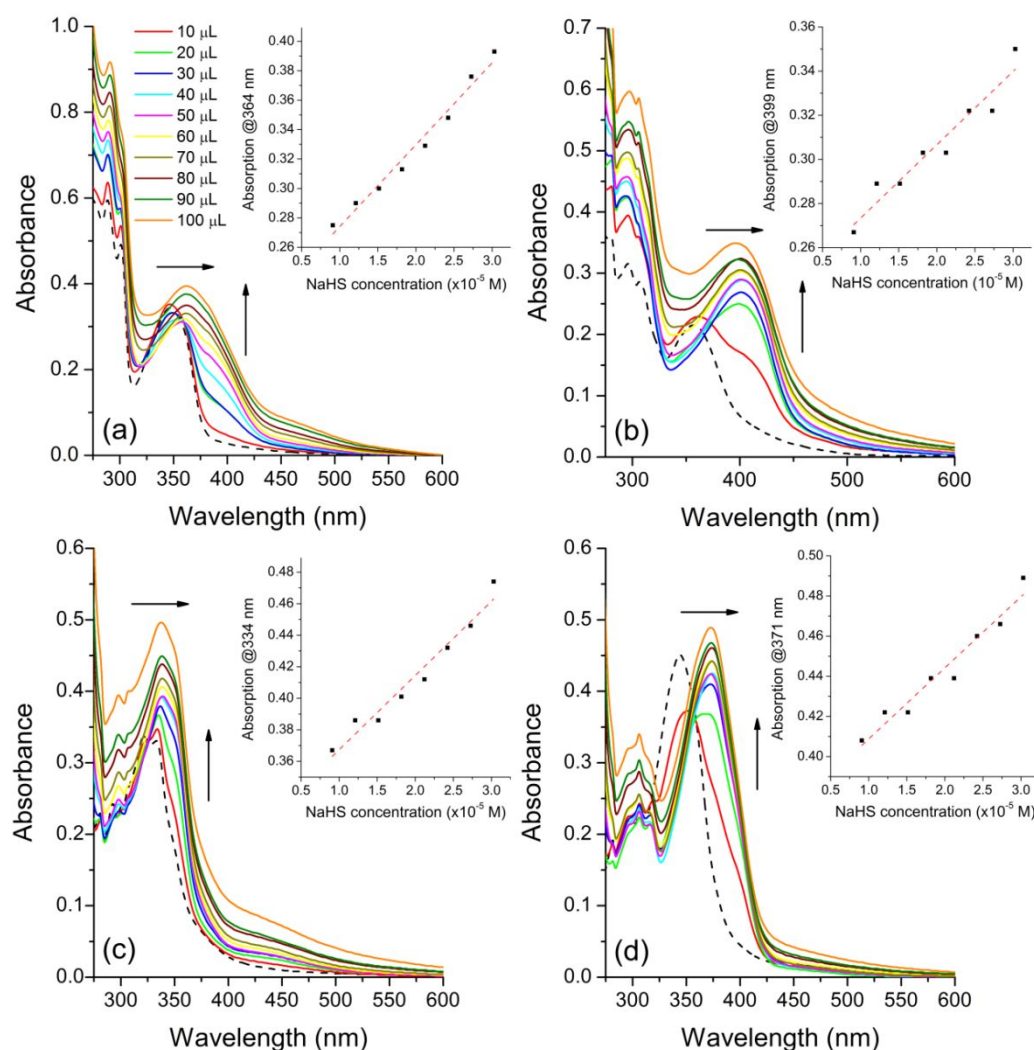


Figure 4. UV-Vis spectra of compounds (a) **6** (2.88×10^{-5} M) and (b) **7** (2.98×10^{-5} M) and (c) **11** (1.98×10^{-5} M) and (d) **12** (1.86×10^{-5} M) upon addition of different amounts (10-100 μL) of NaHS (1.0×10^{-3} M) in ethanol/PBS buffer solution (50/50 v/v, pH=7.4). The dash line is the respective azide in absence of NaHS. The inset presents the respective correlation between the absorption intensity and NaHS concentration at the absorption maxima of the reduced compound.

In order to evaluate the azides **6-7** and **11-12** for H_2S detection by the well-known off-on response presented by azide compounds, fluorescence titrations were also performed (Figure 5). The azides present low fluorescence intensity prior to the addition of NaHS. After the addition of different amounts of NaHS a gradual increase in the fluorescence intensity of the azides was observed, characterizing the off-on response mechanism. Azides **6-7** and **12** presented an linear relationship between fluorescence intensity and NaHS concentration,^{15,57} where azide **6** presented the broader linear range (10-100 μM) if compared to the azides **7** and **12** (20-100 μM). This result indicates that

the fluorescence response of these compounds for NaHS can also be used for the quantitative detection of H₂S. It is worth mentioning that although azide **11** presented an increase on the fluorescence intensity upon addition of NaHS, a linear response was not observed, probably due to the dual fluorescence emission that remains present after addition of 30 μ L of NaHS.

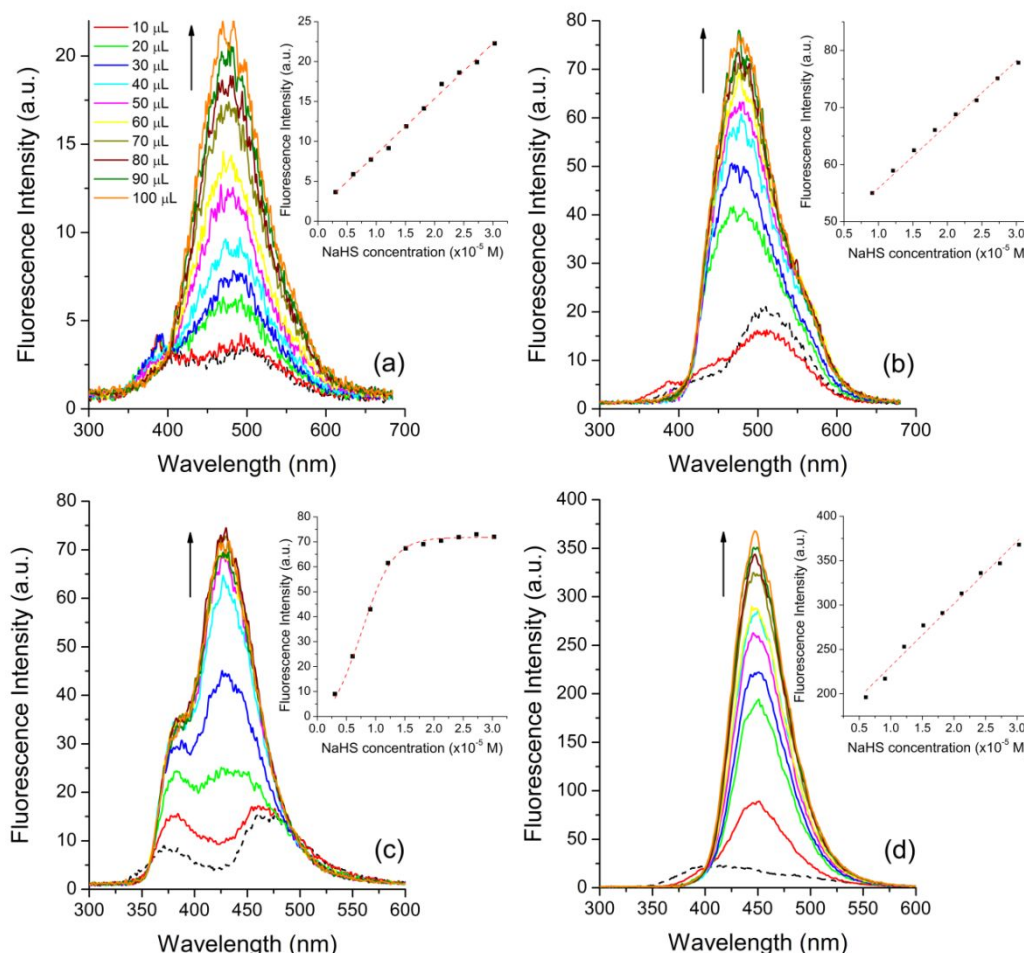


Figure 5. Fluorescence emission spectra of compounds (a) **6** ($\lambda_{\text{exc}}=364$ nm, [2.88×10^{-5} M]) and (b) **7** ($\lambda_{\text{exc}}=399$ nm, [2.98×10^{-5} M]) and (c) **11** ($\lambda_{\text{exc}}=334$ nm, [1.98×10^{-5} M]) and (d) **12** ($\lambda_{\text{exc}}=371$ nm, [1.86×10^{-5} M]) upon addition of different amounts (10–100 μ L) of NaHS (1.0×10^{-3} M) in ethanol/PBS buffer solution (50/50 v/v, pH=7.4) and Exc/Em slits 3.0 nm/3.0 nm. The dash line is the respective azide in absence of NaHS. The inset presents the respective correlation between the fluorescence intensity and NaHS concentration at the emission maxima.

Figure 6 presents the azides **6-7** and **12** in ethanol/PBS buffer solution (50/50, v/v, pH=7.4) under normal light (left) and UV radiation (right). As already observed in

their fluorescence emission profile, in absence of NaHS the solutions of **6-7** are non-fluorescent and **11-12** presents a very weak fluorescence emission, as expected. After addition of NaHS, the azide compounds are converted to the respective amino derivatives, which are fluorescent in solution (bottom right). In order to verify the proposed reaction mechanism, the product of the reaction of compound **7** with NaHS was analyzed by high resolution electrospray mass spectrometry (ESI-HRMS) and we have confirmed the structure of compound **5** as the result of the azide-to-amino reduction ($M+H^+$ m/z 243.0430, see Supporting Information, Figure S41). In addition, time resolved fluorescence spectroscopy (Figure 7 and Table S3) was also used in order to investigate the reaction mechanism in these compounds. The full time decay spectra and the respective residuals are also presented in the ESI (Figures S42-45).

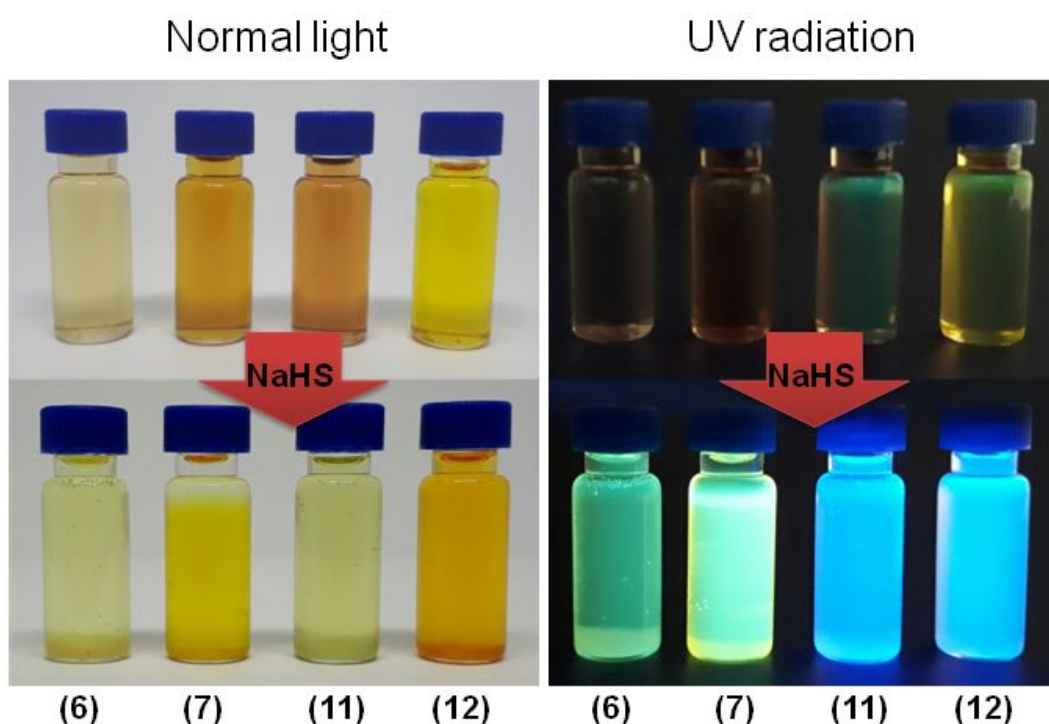


Figure 6. Solutions of azides **6-7** and **11-12** in ethanol/PBS buffer solution (50/50 v/v, pH=7.4) under normal light (left) and UV radiation (right) in absence (top) and in presence (bottom) of NaHS.

The fluorescence decay profile of the studied compounds could be fitted by one-exponential decays with good χ^2 values. It can be observed that in buffered media the azide derivative **7** presents in absence of NaHS one single exponential decay with very short fluorescence lifetime ($\tau \sim 0.05$ ns) almost overlapping to the instrument response function (IRF). However, in presence of the NaHS, a commonly employed H_2S donor,

the fluorescence lifetime becomes 3 times longer ($\tau \sim 0.15$ ns), which can be directly related to the fluorescence lifetime of the reduced compound **5** at the same buffered solution ($\tau \sim 0.18$ ns). A similar value was observed for compound **5** in presence of NaHS ($\tau \sim 0.20$ ns), where any chemical reaction were expected. It is believed that the observed differences to the fluorescence lifetime values can probably be related to the sensibility of the technique in PBS media.

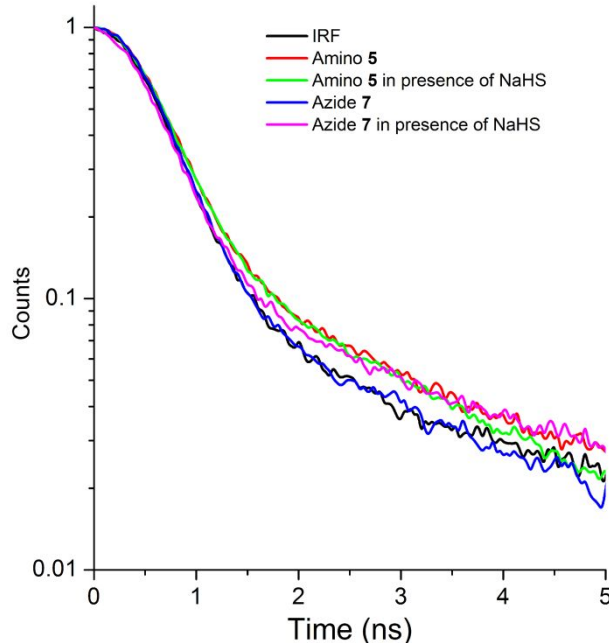


Figure 7. Fluorescence decays of azide **7** and respective amino derivative **5**. [ca. 10^{-5} M]. IRF=instrument response factor.

Based on the previous photophysical results, the reaction kinetics of the synthesized azides upon addition of NaHS were also investigated by analyzing the changes on the UV-Vis (Figure 8) and fluorescence emission (Figure 9) spectra as a function of reaction time. In Figure 8 is presented the evolution of the absorption maxima of the azides in time, where it can be observed that each compound behaves differently. It can be observed that the absorption intensity around 400 nm of azides **6** and **12** decreases after NaHS addition and a new absorption band arises and increases its intensity at 350 nm. For compounds **7** and **11** the absorption intensity increases and shifts upon addition of NaHS. In this process, compounds **11** and **12** presents one isosbestic point located at 363 nm and 377 nm, respectively, suggesting a clean chemical reduction from azide to amino, as already observed in the literature.^{15,57} However, compound **6** presents two isosbestic points (370 nm and 416 nm) in despite of

its absence for compound **7** indicating that for these derivatives an intricate chemical transformation is taking place.

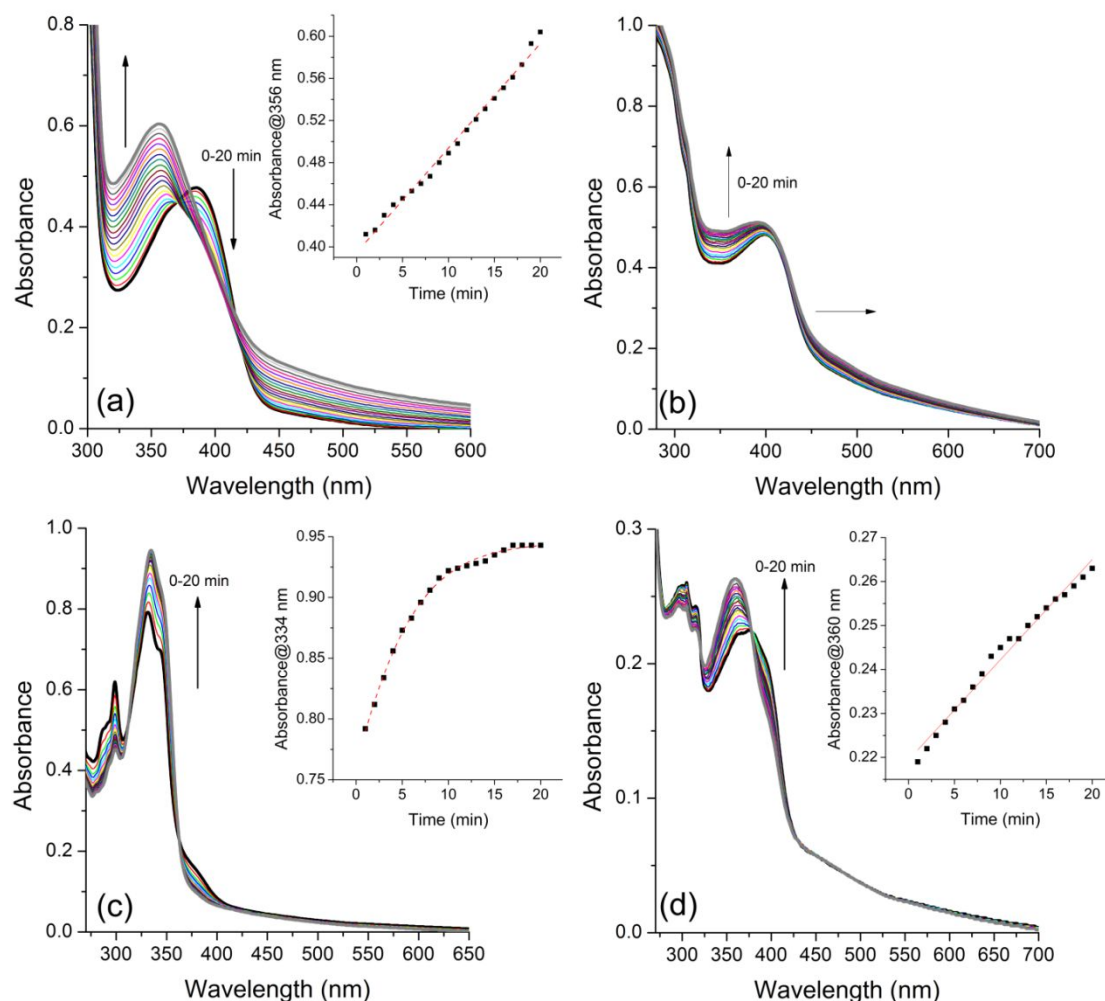


Figure 8. Time dependent UV-Vis absorption spectra of the synthesized azides (a) **6** ($[2.88 \times 10^{-5} \text{ M}]$) and (b) **7** ($[2.98 \times 10^{-5} \text{ M}]$) and (c) **11** ($[1.98 \times 10^{-5} \text{ M}]$) and (d) **12** ($[1.86 \times 10^{-5} \text{ M}]$) upon addition of different amounts (10-100 μL) of NaHS ($1.0 \times 10^{-3} \text{ M}$) in ethanol/PBS buffer solution (50/50 v/v, pH=7.4). The black line is the respective azide in absence of NaHS. The inset presents the respective correlation between the absorption intensity and NaHS concentration.

Figure 9 presents the evolution of the emission maxima of the azides in time. Once again, although these compounds presented significant signal changes in presence of NaHS, it can be observed that each compound shows a particular emission profile. It can be observed that azides **6** and **7** present very low fluorescence intensity, which increases significantly after NaHS addition with large Stokes shift. This last feature is quite interesting for fluorescence imaging applications.⁵⁸ For compounds **11** and **12** a dual fluorescence emission was already present, which increases its intensity

and blue shift the emission maxima at 375 and 435 nm, respectively. However, in general the reaction rate almost has no change with the variation of NaHS concentration after 10 minutes. Compound **6** showed to need longer reaction time to reach the spectra saturation.

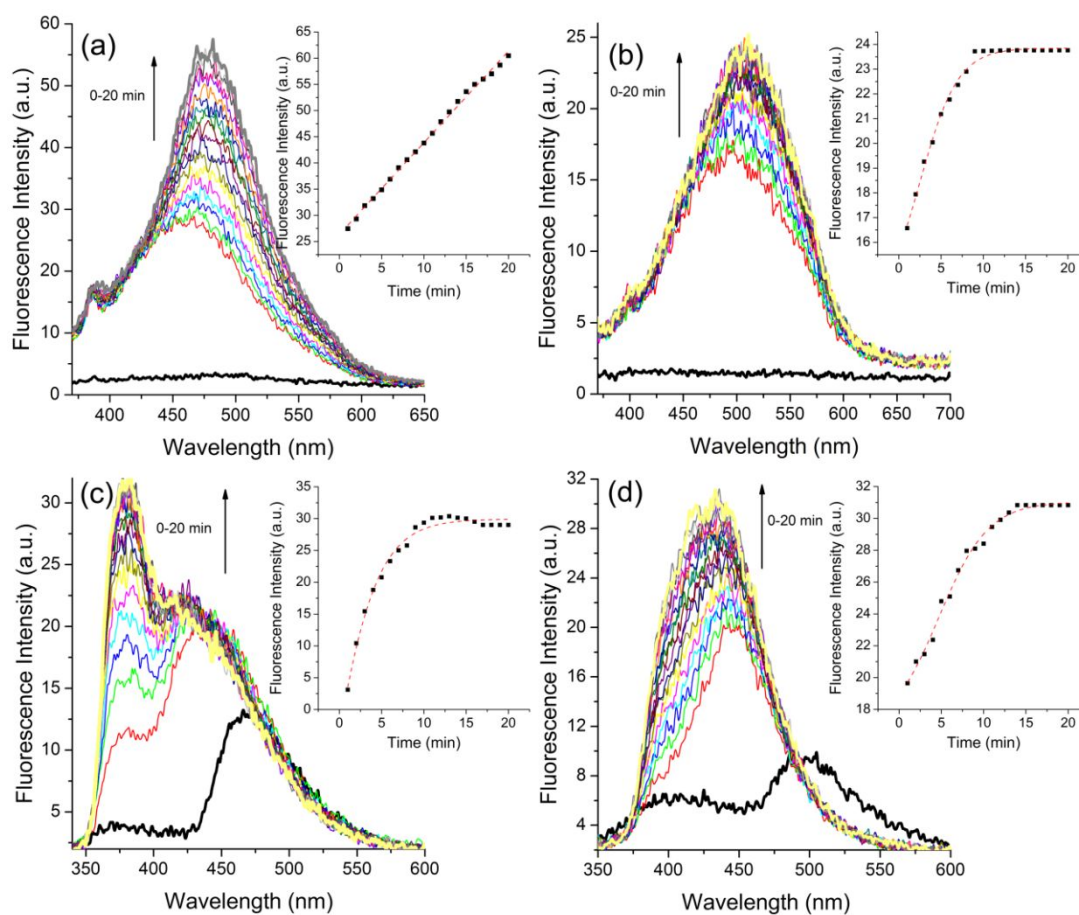


Figure 9. Time dependent fluorescence emission spectra of the synthesized azides (a) **6** ($\lambda_{\text{exc}} = 356$ nm, $[2.88 \times 10^{-5}$ M]) and (b) **7** ($\lambda_{\text{exc}} = 350$ nm, $[2.98 \times 10^{-5}$ M]) and (c) **11** ($\lambda_{\text{exc}} = 334$ nm, $[1.98 \times 10^{-5}$ M]) and (d) **12** ($\lambda_{\text{exc}} = 360$ nm, $[1.86 \times 10^{-5}$ M]) upon addition of different amounts (10-100 μL) of NaHS (1.0×10^{-3} M) in ethanol/PBS buffer solution (50/50 v/v, pH=7.4). The black line is the respective azide in absence of NaHS. The inset presents the respective correlation between the fluorescence intensity and NaHS concentration.

Cell staining

In order to evaluate the efficacy of these probes as H_2S cell markers, the T98G cells were used, in an experiment model using fixed cells. All four compounds (**6-7** and **11-12**) were skilled in cell labeling (Figure 10), demonstrated that the probes are suitable for

H₂S detection, without altering the cells morphology. Considering the 7-AADA nucleus labeling (in blue) and despite that fluorophores containing similar benzazole moieties stain cell nuclei,⁵⁹ it seems that the labeling by the different azide probes (in green) is not specific to any cell structure, resulting in a diffuse cellular marking. It is important to note, as presented in the literature,^{32,38,57,60} that cysteine could be regarded as a precursor to H₂S in the cell imaging assays, so in this work the T98G cells were pre-incubated with cysteine and then incubated with synthesized azides. Also, we performed a control using cells not stained with dyes (7-AAD and azides) and no cells autofluorescence was observed in time exposure and excitation/emission channels used (data not shown).

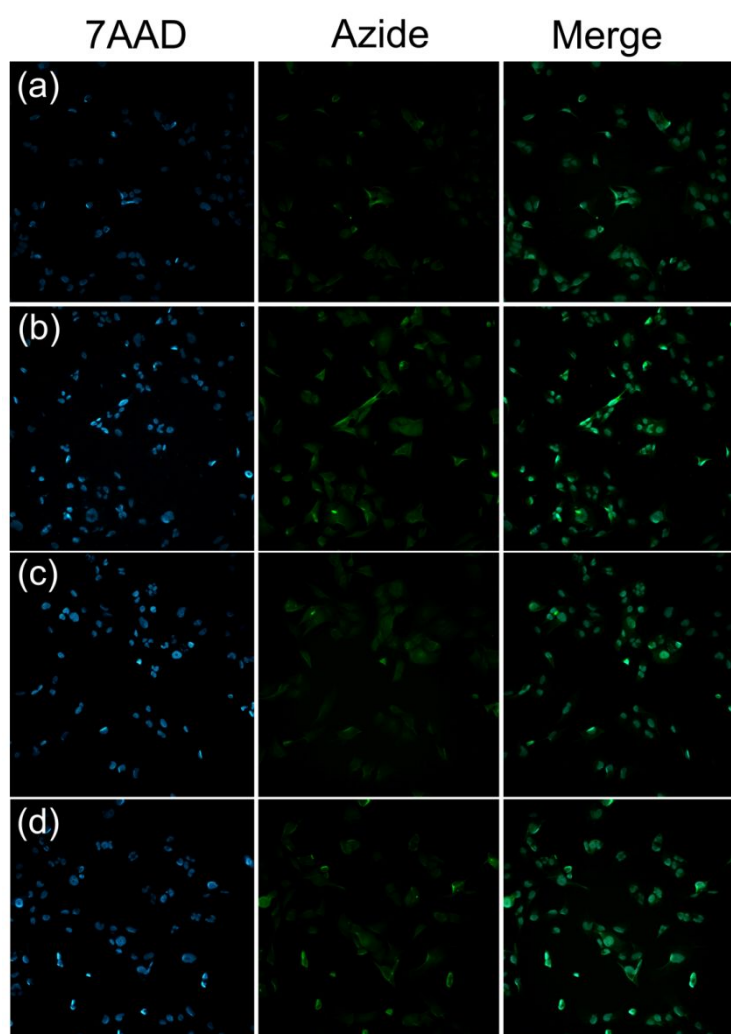


Figure 10. Fluorescence microscopy images of the azides (a) **6**, (b) **7**, (c) **11** and (d) **12** in T98G fixed cells. The first column shows the fluorescence of cells incubated with the nuclear dye 7-AAD, central column show the azide compounds and third column the overlap of the images. Image acquired at 20× as single image field (20× 0.75 NA objective).

Theoretical calculations

The optimized geometry for the ground and the first excited states of azides **6** and **11** in dichloromethane are shown in Table 3. The optimized geometries in acetonitrile and ethanol can be found in Tables S1 and S2 in the SI. It is possible to see, by the experimental emission spectra values, that there are two emitting species: the enol tautomer and the keto tautomer. No significant geometry changes were observed for the enol species when comparing the S₀ and S₁ states for both azides.

Table 3. S₀ and S₁ optimized geometries for azides **6** and **11**, computed at the CAM-B3LYP/cc-pVDZ level in dichloromethane.

	Azide 6	Azide 11
Enol S ₀		
Enol S ₁		
Keto S ₁		

The Figure 11 shows the energies of enol and keto tautomers in ground and first excited states for azide **11** calculated at the CAM-B3LYP/cc-pVDZ level in acetonitrile. The enol tautomer of azide **11** is 0.93 eV more stable than the keto tautomer in the S₀. Because of this great energy difference, the energy is absorbed by the enol tautomer, as experimentally observed. The energy of keto tautomer in the first excited state is only 0.06 eV less stable than enol conformer, and because of this small energy difference, the enol conformer is easily converted into its tautomer.

In Table 4, the NTOs for the first transition of azides **6** and **11** are shown for three different solvents. We can observe that the NTOs coefficients in the ground and the first excited states look like π -type orbitals for both azides in all considered solvents. Thus, it was assumed that $\pi \rightarrow \pi^*$ transitions were occurring for both structures. The azide **6** LUMO orbital in dichloromethane is delocalized in the molecule, but in ethanol and acetonitrile it cannot be observed.

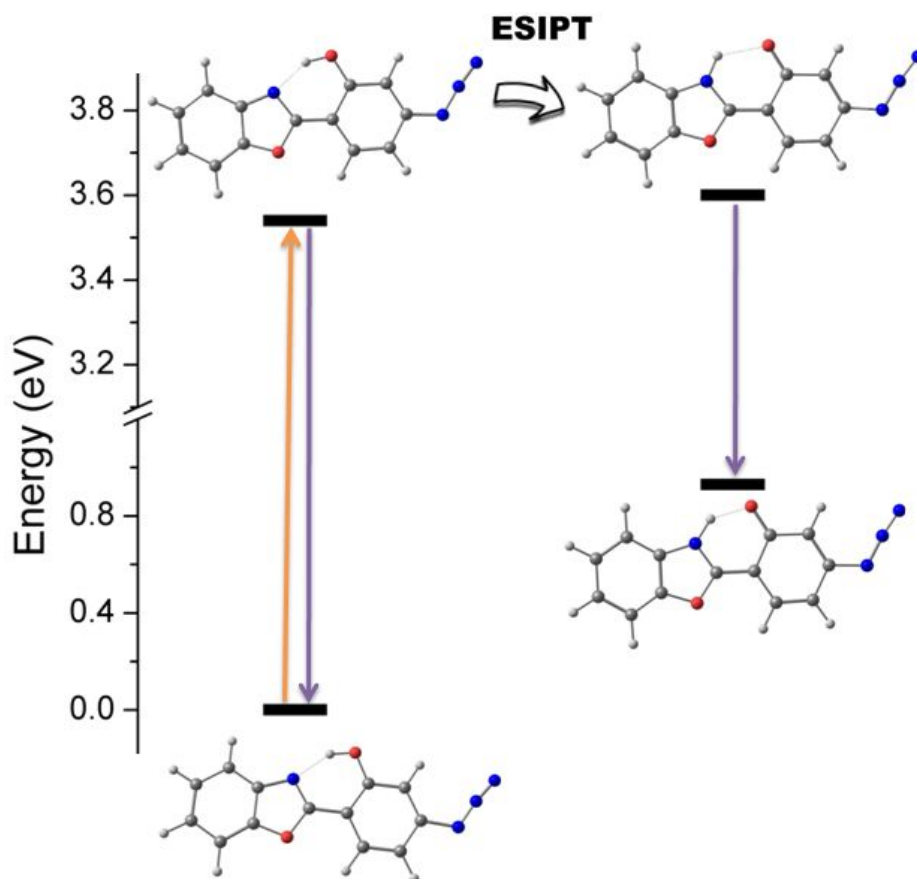


Figure 11. Enol and keto tautomers energies in ground and first excited state for azide **11** computed at the CAM-B3LYP/cc-pVDZ level in acetonitrile.

The calculated photophysical data are shown in Table 5. The CAM-B3LYP/cc-pVDZ values for absorption and emission wavelength are in good agreement with the experimental data.

Table 4. NTOs orbitals involved in the first transition for azides **6** and **11** computed at the CAM-B3LYP/jun-cc-pVTZ level in acetonitrile (CH₃CN), dichloromethane (DCM) and ethanol (EtOH).

Azide	Solvent	S ₀	S ₁
6	CH ₃ CN		
	DCM		
	EtOH		
11	CH ₃ CN		
	DCM		
	EtOH		

Table 5. Computed photophysical data at the CAM-B3LYP/jun-cc-pVTZ level for azides **6** and **11** in acetonitrile (CH₃CN), dichloromethane (DCM) and ethanol (EtOH). Where λ_{abs} is the wavelength of absorption, λ_{em} is the emission wavelength, f_{abs} is the absorption oscillator strength, f_{em} is the emission oscillator strength and $\mu(1 \rightarrow 2)$ is the transition dipole moment for the first excitation.

Azide	6			11		
Solvent	DCM	EtOH	CH ₃ CN	DCM	EtOH	CH ₃ CN
λ_{abs}	320	319	319	311	310	309
f_{abs}	0.4082	0.0003	0.0002	1.0991	1.0800	1.0741
$\lambda_{\text{em (enol)}}$	382	385	385	377	382	382
$f_{\text{em (enol)}}$	0.5862	0.6260	0.6334	1.4464	1.1963	1.5050
$\lambda_{\text{em (keto)}}$	464	469	469	415	417	418
$f_{\text{em (keto)}}$	0.4649	0.4761	0.4804	0.6854	0.7355	0.7445
$\mu(1 \rightarrow 2)$	4.3029	0.0026	0.0026	11.2408	11.0075	10.9378

However, the main question to be answered in this work, almost absent in the literature, is "why does azide **11** show more intense fluorescence emission than azide **6**?". In order to answer the question, the transition dipole moment (TDM) values of these molecules (Table 5) must be taken into account. The TDM for azide **11** is greater than that of azide **6**, therefore, azide **11** has a greater oscillator strength, since the TDM is proportional to the square of oscillator strength, as shown by the equation (1):

$$\mu^2 = \frac{3e^2h}{8\pi^2m_e\nu} \times f \quad (1)$$

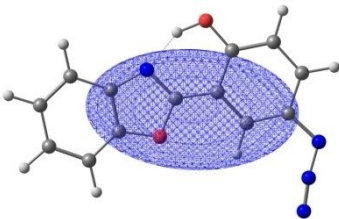
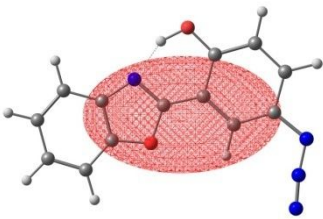
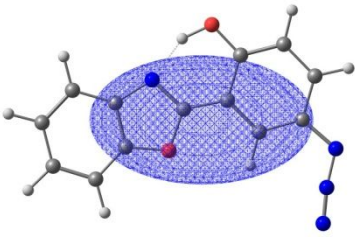
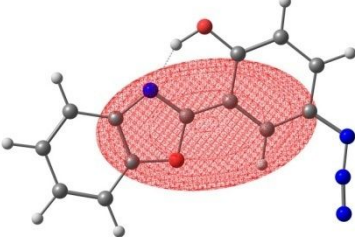
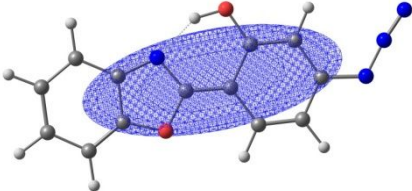
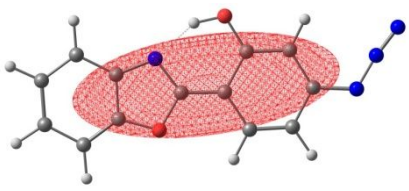
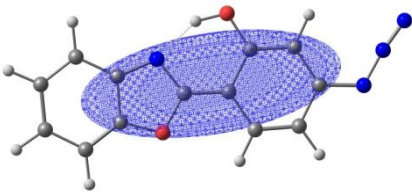
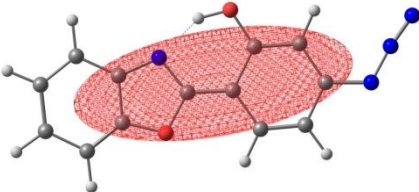
where μ is the dipole moment, e is the electron charge, h is the Planck constant, m_e is the electron mass, ν is the wavenumber and f is the oscillator strength.

We can assume that the azide **11** is able to absorb more energy than azide **6**, thus, a more intense fluorescence emission is observed. This photophysical behavior can also be related to the TDM value of this molecule in dichloromethane, which is much higher than in ethanol and acetonitrile.

A quantitative assessment of the local excitation and charge transfer to the excited states was performed and shows that no charge transfer is present in these

systems, but only local excitation. The overlap integral between the centroids of charges (C+ and C-) before and after transition, obtained from the charge transfer diagnostic index (D_{CT}) were computed in acetonitrile and ethanol. The D_{CT} represents the distance between the centroids of charges obtained before and after the transition. After the transition, the electronic density tends to be relocated considering the donors and acceptors groups in the molecule. The results of D_{CT} analysis are shown in Table 6. For both azides, the centroids of charges before and after transition are localized in the same region with no displacement between the centroids, excluding the charge transfer chance for these azides.

Table 6. D_{CT} overlap integral between centroids of charges obtained before and after the transition computed with Multiwfn program for azides **6** and **11** in acetonitrile and ethanol.

Azide	Solvent	C+	C-
6	CH ₃ CN		
	EtOH		
11	CH ₃ CN		
	EtOH		

Conclusions

In summary, we presented here the synthesis of four novel azide based benzoxazoles achieved via diazonium salts formation from the respective amino precursors followed by addition of sodium azide (NaN_3) through an unimolecular nucleophilic substitution reaction ($\text{S}_{\text{N}}1$). The obtained compounds present absorption maxima located in the UV region (330-360 nm) related to fully spin and symmetry allowed $^1\pi\rightarrow\pi^*$ electronic transitions. A low intense or almost absent fluorescence emission bands, tailored by the azide group position were observed in the visible region. All studied compounds presented significant changes on their photophysics in presence of NaHS, which allowed apply these compounds as optical sensors for H_2S in solution. The methodology employed was the reduction of azides to amines using H_2S , resulting in an off-on response fluorescence mechanism. From the theoretical calculations, it was observed that the π frontier orbitals are involved in the first transition for azides considered, indicating $^1\pi\rightarrow\pi^*$ transition is taking place. Furthermore, these excitations are localized, indication that charge-transfer are not occurring, which has proved by the D_{CT} descriptor. The fluorescence quenching observed in the azide **6**, differently than the photoinduced electron transfer process (PET), discussed in the literature, and was explained by the small transition dipole moment for the first transition. Finally, the fluorescence imaging experiments in T98G cells indicate its potential to probe H_2S in fixed cells. Since these molecules were efficient for the labeling of biological systems, further experiments using living cells should be conducted in a next step of this study and this results will be reported in due course.

Experimental Section

General Information. All reagents were used as received. The solvents were purchased from commercial sources and purified according to procedures in the literature.⁶¹ The reactions were monitored by Thin-Layer Chromatography (TLC) using Silica Gel 60 F254. Fourier transform infrared (FTIR) spectra ($600\text{--}4000\text{ cm}^{-1}$) were recorded on a Varian model 640-IR, with a resolution of 4 cm^{-1} using KBr pellets. Proton and Carbon nuclear magnetic resonance spectra (^1H and $^{13}\text{C}\{^1\text{H}\}$ NMR) were recorded in CDCl_3 at 300 and 75.5 MHz, respectively. Proton nuclear magnetic resonance spectra (^1H NMR) was recorded in CDCl_3 or $\text{DMSO-}d_6$ at 300 or 400 MHz. Proton-decoupled carbon nuclear magnetic resonance spectra ($^{13}\text{C}\{^1\text{H}\}$ NMR) was recorded in CDCl_3 or $\text{DMSO-}d_6$ at 75.5 or 101 MHz. The chemical shifts (δ) are reported in parts per million

(ppm) relative to TMS (0.00 ppm), and the coupling constants J are reported in hertz (Hz). Melting points were obtained on a QUIMIS model Q340S and are uncorrected. In the photophysical studies, spectroscopic-grade solvents were used. The UV-Vis spectra were recorded on a Shimadzu UV-2450 spectrophotometer, and the steady-state fluorescence spectra were measured on a Shimadzu spectrofluorometer model RF-5301PC. The quantum yield of the fluorescence signals (Φ_{FL}) was obtained with the dilute optical method using spectroscopic-grade solvents. Quinine sulfate in H₂SO₄ (0.5 mol L⁻¹) (Φ_{FL} =0.55) was used as the quantum yield standard.⁶² Time resolved fluorescence curves were performed in PBS buffer using an EasyLife V spectrophotometer (Optical Building Blocks). All measurements were performed at room temperature. The decay curves were analysed using EasyLife V software (OBB). A nonlinear least square method was employed for the fit of the decay to a sum of exponentials. The value of χ^2 , respective residuals and the autocorrelation function were used to determine the quality of the proposed fit.

Synthesis. The benzazole precursors **4-5** and **9-10** were obtained by a condensation reaction between the ortho-substituted anilines **1-2** and the 5- or 4-aminosalicylic acids (**3** and **8**), respectively in polyphosphoric acid (PPA) at 170°C for 5h (Scheme S1).^{63,64} The progress of the chemical reaction was monitored by TLC. The solution was neutralized with NaHCO₃ (10%), the precipitate was filtered and dried at 60°C. The purification was performed by column chromatography using dichloromethane as eluent. The azides **6-7** and **11-12** were synthesized using the reaction of formation of diazonium salts from the respective aromatic amines **4-5** or **9-10**. The first step is the amino group diazotization by reaction with sodium nitrite (NaNO₂) in aqueous HCl. During this step, the mixture temperature was maintained at 0°C in order to stabilize the resulting diazonium salt, which could improve reaction yields. After the formation of the diazonium salt, sodium azide (NaN₃) was added and the reaction to obtain the respective azides takes place through an unimolecular nucleophilic substitution reaction (S_N1). After 2h under stirring, the final solution was neutralized with NH₄OH, extracted with ethyl acetate and concentrated under reduced pressure to yield the desirable azides in satisfactory yields, which were used without further purification.

General procedure for the synthesis of precursors 4-5 and 9-10. An equimolar mixture of o-aminophenol (**1**) (2.8 g, 26.12 mmol) or o-aminothiophenol (**2**)

(2.76 mL, 26.12 mmol) and 5-aminosalicylic acid (**3**) or 4-aminosalicylic acid (**8**) (4.0 g, 26.12 mmol) in polyphosphoric acid (60 mL) was stirred at 170°C for 5 h. After cooling, the mixture was poured onto ice under vigorous stirring. The solution was neutralized with NaHCO₃. The precipitate was filtered, washed with water and dried at 60°C. The solid was purified by column chromatography using dichloromethane as eluent.⁵⁴

2-(5'-Amino-2'-hydroxyphenyl)benzoxazole (4). Yield: 71% (0.294 g). Melting point: 173-175°C. FTIR (KBr, cm⁻¹): 3405 (ν_{as} NH₂), 3250 (ν_s NH₂), 1630 and 1548 (ν C=C). ¹H NMR (300 MHz, DMSO-*d*₆) δ (ppm): 10.42 (s, 1H, OH), 7.81 (m, 2H), 7.44 (m, 2H), 7.26 (d, 1H, J=2.3 Hz), 6.84 (m, 2H), 4.96 (s, 2H). ¹³C{¹H} NMR (75.5 MHz, DMSO-*d*₆) δ (ppm): 162.8, 149.3, 148.6, 141.7, 139.6, 125.6, 125.2, 121.3, 119.0, 117.6, 110.9, 110.4, 109.6.

2-(5'-Amino-2'-hydroxyphenyl)benzothiazole (5). Yield: 53% (0.271 g). Melting point: 196-198°C. FTIR (KBr, cm⁻¹): 3497 (ν_{as} N-H), 3325 (ν_s N-H), 3000 (ν_{arom} C-H), 1620 and 1470 (ν C=C_{arom}). ¹H NMR (300 MHz, DMSO-*d*₆) δ (ppm): 10.72 (s, 1H, OH), 8.12-7.40 (m, 4H, H1, H2, H3, H4), 7.37-7.36 (d, 1H, J=2.7 Hz), 6.85-6.83 (d, 1H, J=8.7 Hz), 6.77-6.76 and 6.74-6.73 (2d, 1H, J=2.7 Hz and J=8.8 Hz), 4.8 (s, 2H). ¹³C{¹H} NMR (75.5 MHz, DMSO-*d*₆) δ (ppm): 166.3, 151.6, 147.8, 141.5, 134.0, 126.4, 125.0, 121.9, 121.8, 119.9, 117.8, 117.6, 112.0.

2-(4'-Amino-2'-hydroxyphenyl)benzoxazole (9). Yield: 44% (0.182 g). Melting point: 226-228°C. FTIR (KBr, cm⁻¹): 3493 (ν_{as} N-H), 3386 (ν_s N-H), 3000 (ν_{arom} C-H), 1620 and 1470 (ν C=C_{arom}). ¹H NMR (400 MHz, CDCl₃) δ (ppm): 10.95 (s, 1H), 7.76-7.71 (m, 1H), 7.63-7.58 (m, 1H), 7.42-7.36 (m, 3H), 6.99 (d, 1H, J=4.1 Hz), 6.87 (dd, 1H, J=8.7 Hz and J=2.8 Hz), 3.56 (s, 2H). ¹³C{¹H} NMR (101 MHz, CDCl₃) δ (ppm): 163.6, 160.6, 151.7, 148.9, 140.4, 128.6, 124.6, 124.3, 118.5, 110.2, 107.3, 101.5, 101.5.

2-(4'-Amino-2'-hydroxyphenyl)benzothiazole (10). Yield: 33% (0.169 g). Melting point: 211-213°C. FTIR (KBr, cm⁻¹): 3473 (ν_{as} N-H), 3376 (ν_s N-H), 3000 (ν_{arom} C-H), 1620 and 1470 (ν C=C_{arom}). ¹H NMR (400 MHz, CDCl₃) δ (ppm): 12.66 (s, 1H), 7.90 (d, 1H, J=8.1 Hz), 7.86 (d, 1H, J=7.9 Hz), 7.49-7.43 (m, 2H), 7.38-7.33 (m, 1H), 6.34 (d, 1H, J=2.2 Hz), 6.28 (dd, 1H, J=8.4 Hz and J=2.3 Hz), 4.05 (s, 2H). ¹³C{¹H}

NMR (101 MHz, CDCl_3) δ (ppm): 169.6, 160.1, 152.2, 150.9, 132.3, 130.0, 126.4, 124.6, 121.4, 121.3, 108.5, 107.2, 101.7.

General procedure for the synthesis of azides 6-7 and 11-1. In a 50 mL round bottom flask under an ice bath containing 2.0 mmol of the benzazole precursors **4-5** (452 and 485 mg, respectively) or **9-10** (452 and 485 mg, respectively) and a $\text{HCl}:\text{H}_2\text{O}$ (3:1) solution (15 mL) it was added dropwise a NaNO_2 (0.166 g, 2.4 mmol) solution (1 mL). The reaction mixture was stirred under ice bath for 30 min. After this time, NaN_3 was added (0.260 g, 4.0 mmol). The reaction mixture was stirred at room temperature for 2h. After this time, the solution was neutralized with NH_4OH , extracted with ethyl acetate (3x20 mL) and concentrated under reduced pressure to yield the respective product.

2-(5'-Azido-2'-hydroxyphenyl)benzoxazole (6). Yield: 79% (0.464 g). Melting point: 143-145°C. FTIR (KBr, cm^{-1}): 3056 (ν_{arom} C-H), 2117 (ν -N=N=N), 1553 and 1471 (ν C=C_{arom}). ^1H NMR (400 MHz, CDCl_3) δ (ppm): 11.37 (s, 1H), 7.77-7.72 (m, 1H), 7.67-7.61 (m, 2H), 7.45-7.39 (m, 2H), 7.16-7.07 (m, 2H). $^{13}\text{C}\{^1\text{H}\}$ NMR (101 MHz, CDCl_3) δ (ppm): 161.9, 156.0, 149.1, 139.8, 131.5, 125.8, 125.2, 124.4, 119.4, 118.9, 116.6, 111.2, 110.8. HRMS (ESI-TOF) m/z : $[\text{M}+\text{H}]^+$ Calcd for $\text{C}_{13}\text{H}_9\text{N}_4\text{O}_2$ 253.0726; Found 253.0723.

2-(5'-Azido-2'-hydroxyphenyl)benzothiazole (7). Yield: 70% (0.456 g). Melting point: 147-149°C. FTIR (ATR, cm^{-1}): 3086 (ν O-H), 2098 (ν -N=N=N), 1613 and 1513 (ν C=C_{arom}). ^1H NMR (400 MHz, CDCl_3) δ (ppm): 12.43 (s, 1H), 7.99 (d, 1H, $J=8.1$ Hz), 7.91 (d, 1H, $J=7.9$ Hz), 7.56-7.49 (m, 1H), 7.46-7.40 (m, 1H), 7.26 (d, 1H, $J=2.5$ Hz), 7.11-7.05 (m, 2H). $^{13}\text{C}\{^1\text{H}\}$ NMR (101 MHz, CDCl_3) δ (ppm): 161.9, 156.0, 149.1, 139.8, 131.5, 125.8, 125.2, 124.4, 119.4, 118.9, 116.6, 111.2, 110.8. HRMS (ESI-TOF) m/z : $[\text{M}+\text{H}]^+$ Calcd for $\text{C}_{13}\text{H}_9\text{N}_4\text{OS}$ 269.0497; Found 269.0477.

2-(4'-Azido-2'-hydroxyphenyl)benzoxazole (11). Yield: 90% (0.464 g). Melting point: 111-112°C. FTIR (ATR, cm^{-1}): 3056 (ν O-H), 2118 (ν -N=N=N), 1644 and 1573 (ν C=C_{arom}). ^1H NMR (300 MHz, CDCl_3) δ (ppm): 11.60 (s, 1H), 7.98 (d, 1H, $J=7.7$ Hz), 7.67 (d, 2H, $J=7.9$ Hz), 7.40 (s, 2H), 6.79 (s, 1H), 6.68 (d, 1H, $J=7.2$ Hz). $^{13}\text{C}\{^1\text{H}\}$ NMR (101 MHz, CDCl_3) δ (ppm): 162.3, 159.9, 149.0, 139.9, 128.5, 125.4, 125.1, 119.1, 110.9,

110.6, 107.6, 107.4. HRMS (ESI-TOF) m/z : $[M+H]^+$ Calcd for $C_{13}H_9N_4O_2$ 253.0726; Found 253.0726.

2-(4'-Azido-2'-hydroxyphenyl)benzothiazole (12). Yield: 89% (0.456 g). Melting point: 132-134°C. FTIR (ATR, cm^{-1}): 3077 (ν O-H), 2117 (ν -N=N=N), 1653 and 1573 (ν C=C_{arom}). 1H NMR (400 MHz, $CDCl_3$) δ (ppm): 12.79 (s, 1H), 7.96 (d, 1H, $J=7.7$ Hz), 7.88 (d, 1H, $J=7.5$ Hz), 7.61 (d, 1H, $J=8.4$ Hz), 7.54-7.49 (m, 1H), 7.45-7.38 (m, 1H), 6.74 (d, 1H, $J=2.2$ Hz), 6.59 (dd, 1H, $J=8.4$ Hz and 2.2 Hz). $^{13}C\{^1H\}$ NMR (75 MHz, $CDCl_3$) δ (ppm): 162.3, 159.9, 149.0, 145.2, 139.9, 128.5, 125.4, 125.1, 119.1, 110.9, 110.6, 107.5, 107.3. HRMS (ESI-TOF) m/z : $[M+H]^+$ Calcd for $C_{13}H_9N_4OS$ 269.0497; Found 269.0493.

H₂S detection. The study of detection of H₂S with the azides **6-7** and **11-12** was performed using a solution of ethanol with concentration in the range of 10^{-5} M. To these solutions were added different amounts (0-100 μ M) of NaHS (1.0×10^{-3} M) in ethanol/PBS buffer solution (50/50, v/v, pH = 7.4) at room temperature.

Theoretical calculations. The geometry optimizations and vibrational frequencies were evaluated using DFT and the vertical transitions were computed using TD-DFT (Time-Dependent Density Functional Theory). The CAM-B3LYP⁶⁵ functional was chosen to perform all the calculations. This functional was chosen because it shows good results for a series of applications, especially in TD-DFT calculations, as reported in the literature.⁶⁶⁻⁶⁸ All the geometry optimizations were carried out using the Dunning cc-pVDZ⁶⁹ basis set, and a jun-cc-pVTZ basis set was used in TD-DFT calculations. The use of *jun*- basis functions was because it is necessary diffuse functions for a good description of excited states. These basis function were chosen since they have a lower computational cost than *aug*- type base functions, since *jun*- basis functions are constructed by reducing diffuse functions of *aug*- basis functions.⁷⁰ Since the sulphurous analogues **7** and **12** presented similar photophysical features than the oxygenated ones, the calculations were performed only for the azides **6** and **11**. The solvent effect was considered in all calculation using PCM (Polarizable Continuum Model), and the solvents considered were acetonitrile (CH_3CN), dichloromethane (DCM) and ethanol (EtOH).⁷¹ The NTOs (Natural Transition Orbital) were computed. NTOs drastically simplify the orbital analysis by providing a compact representation of the transition

density matrix.⁷² All the calculations described above were computed using the Gaussian 16 package.⁷³ In order to verify if the molecules undergo charge transfer, the analysis with D_{CT} descriptor⁷⁴ has been carried out using Multiwfn program.⁷⁵ All images were rendered with Chemcraft software.⁷⁶

Cell Culture. The glioblastoma multiform T98G cells were acquired by American Type Culture Collection® (ATCC). The cells were grown in Dulbecco's modified Eagle's medium (Gibco™ DMEM, Life Technology, NY, USA) supplemented with 10% heat-inactivated fetal bovine serum (Gibco™ FBS, Life Technology, NY, USA), 100 units ml⁻¹ penicillin and 100 g ml⁻¹ streptomycin at 37°C in a humidified atmosphere with 5% CO₂.

Fluorescence Response in Biological System. In order to investigate the azides as optical sensors, cells (1.0×10^4 cells) grown on 96-well plates were fixed in paraformaldehyde (3.7%), washed with PBS, permeabilized in Triton X-100 (0.01%) and incubated with cysteine (100 μM, 30 min, 37°C). Then, the cells were washed with PBS and incubated with the azides **6-7** or **11-12** (10 mM) for 30 min at 37°C. The 7-AAD was used to counteract the nucleus, according to manufacturer's recommendations (BD Biosciences, San Diego, CA). After, the cells were imaged in InCell analyzer 2200 (GE Healthcare Life Sciences, Piscataway, NJ, USA) at 390/18 nm excitation and 432.5/48 emission to azides and 597/45 excitation and 542/27 nm emission to 7-AAD.

Supporting Information:

The Supporting Information is available free of charge on the ACS Publications website. Copies of NMR spectra for all compounds, additional photophysical and theoretical data.

Acknowledgements

The authors would like to acknowledge FAPERGS (17/2551-0000968-1), CNPq and Coordenação de Aperfeiçoamento de Pessoal de Nível Superior - Brasil (CAPES) - Finance Code 001 for the financial support. Special thanks for M.Sc. Luana Silva for HRMS data.

References

1. Evans, C. L. The Toxicity of Hydrogen Sulphide and other Sulphides. *Quart. J. Exp. Physiol.* **1967**, *52*, 231-248.
2. Zhi, G.; Chen, G.; Zeng, G.; Li, Z.; Chen, A.; Wang, J.; Jiang, L. Fluorescence Chemosensors for Hydrogen Sulfide Detection in Biological Systems. *Analyst* **2015**, *140*, 1772-1786.
3. Li, J.; Yin, C.; Huo, F. Chromogenic and Fluorogenic Chemosensors for Hydrogen Sulfide: Review of Detection Mechanisms Since the Year 2009. *RSC Adv.* **2015**, *5*, 2191-2206.
4. Pandey, S. K.; Kim, K. H.; Tang, K. T. A Review of Sensor-Based Methods for Monitoring Hydrogen Sulfide. *Trends Anal. Chem.* **2012**, *32*, 87-99.
5. Lippert, A. R. Designing Reaction-Based Fluorescent Probes for Selective Hydrogen Sulfide Detection. *J. Inorg. Biochem.* **2014**, *133*, 136-142.
6. Guidotti, T. L. Hydrogen Sulfide: Advances in Understanding Human Toxicity. *Int. J. Toxicol.* **2010**, *29*, 569-581.
7. Abe, K.; Kimura, H. The Possible Role of Hydrogen Sulfide as an Endogenous Neuromodulator. *J. Neurosci.* **1996**, *16*, 1066-1071.
8. Mustafa, A. K.; Sikka, G.; Gazi, S. K.; Steppan, J.; Jung, S. M.; Bhunia, A. K.; Barodka, V. M.; Gazi, F. K.; Barrow, R. K.; Wang, R.; Amzel, L. M.; Berkowitz, D. E.; Snyder, S. H. Hydrogen Sulfide as Endothelium-Derived Hyperpolarizing Factor Sulphydrates Potassium Channels. *Circ. Res.* **2011**, *109*, 1259-1268.
9. Papapetropoulos, A.; Pyriochou, A.; Altaany, Z.; Yang, G.; Marazioti, A.; Zhou, Z.; Jeschke, M. G.; Branski, L. K.; Herndon, D. N.; Wang, R.; Szabó, C. Hydrogen Sulfide is an Endogenous Stimulator of Angiogenesis. *Proc. Natl. Acad. Sci. USA* **2009**, *106*, 21972-21977.
10. Szabó, C.; Papapetropoulos, A. Hydrogen Sulphide and Angiogenesis: Mechanisms and Applications. *Br. J. Pharmacol.* **2011**, *164*, 853-865.
11. Olson, K. R.; Dombkowski, R. A.; Russel, M. J.; Doellman, M. M.; Head, S. K.; Whitfield, N. L.; Madden, J. A. Hydrogen Sulfide as an Oxygen Sensor/Transducer in Vertebrate Hypoxic Vasoconstriction and Hypoxic Vasodilation. *J. Exp. Biol.* **2006**, *209*, 4011-4023.
12. Peng, Y. J.; Nanduri, J.; Raghuraman, G.; Souvannakitti, D.; Gadalla, M. M.; Kumar, G. K.; Snyder, S. H.; Prabhakar, N. R. H₂S Mediates O₂ Sensing in the Carotid Body. *Proc. Natl. Acad. Sci. USA* **2010**, *107*, 10719-10724.

13. Lee, M.; Schwab, C.; Yu, S.; McGeer, E.; McGeer, P. L. Astrocytes Produce the Antiinflammatory and Neuroprotective Agent Hydrogen Sulfide. *Neurobiol. Aging* **2009**, *30*, 1523-1534.
14. Fu, M.; Zhang, W.; Wu, L.; Yang, G.; Li, H.; Wang, R. Hydrogen Sulfide (H₂S) Metabolism in Mitochondria and Its Regulatory Role in Energy Production. *Proc. Natl. Acad. Sci. USA* **2012**, *109*, 2943-2948.
15. Xiang, K.; Liu, Y.; Li, C.; Tian, B.; Tong, T.; Zhang, J. A. A Colorimetric and Ratiometric Fluorescent Probe With a Large Stokes Shift for Detection of Hydrogen Sulfide. *Dyes Pigm.* **2015**, *123*, 78-84.
16. Eto, K.; Asada, T.; Arima, K.; Makifuchi, T.; Kimura, H. Brain Hydrogen Sulfide is Severely Decreased in Alzheimer's Disease. *Biochem. Biophys. Res. Commun.* **2002**, *293*, 1485-1488.
17. Kamoun, P.; Belardinelli, M. C.; Chabli, A.; Lallouchi, K.; Chadeaux-Vekemans, B. Endogenous Hydrogen Sulfide Overproduction in Down Syndrome. *Am. J. Med. Genet. A* **2003**, *116*, 310-311.
18. Fiorucci, S.; Antonelli, E.; Mencarelli, A.; Orlandi, S.; Renga, B.; Rizzo, G.; Distrutti, E.; Shah, V.; Morelli, A. The Third Gas: H₂S Regulates Perfusion Pressure in Both the Isolated and Perfused Normal Rat Liver and in Cirrhosis. *Hepatology* **2005**, *42*, 539-548.
19. Hartle, M. D.; Pluth, M. D. A Practical Guide to Working with H₂S at the Interface of Chemistry and Biology. *Chem. Soc. Rev.*, **2016**, *45*, 6108-6117.
20. Lawrence, N. S.; Davis, J.; Jiang, L.; Jones, T. G. J.; Davies, S. N.; Compton, R. G. The Electrochemical Analog of the Methylene Blue Reaction: A Novel Amperometric Approach to the Detection of Hydrogen Sulfide. *Electroanalysis* **2000**, *12*, 1453-1460.
21. Spilker, B.; Randhahn, J.; Grabow, H.; Beikirch, H.; Jeroschewski, P. New Electrochemical Sensor for the Detection of Hydrogen Sulfide and Other Redox Active Species. *J. Electroanal. Chem.* **2008**, *612*, 121-130.
22. Bérubé, P. R.; Parkinson, P. D.; Hall, E. R. Measurement of Reduced Sulphur Compounds Contained in Aqueous Matrices by Direct Injection Into a Gas Chromatograph with a Flame Photometric Detector. *J. Chromatogr. A* **1999**, *830*, 485-489.
23. Kato Jr., E. T.; Yoshida, C. M. P.; Reis, A. B.; Melo, I. S.; Franco, T. T. Fast Detection of Hydrogen Sulfide using a Biodegradable Colorimetric Indicator System. *Polym. Int.* **2011**, *60*, 951-956.

24. Yu, F.; Han, X.; Chen, L. Fluorescent Probes for Hydrogen Sulfide Detection and Bioimaging. *Chem. Commun.*, **2014**, *50*, 12234-12249.
25. Ren, T. B.; Xu, W.; Zhang, Q. L.; Zhang, X. X.; Wen, S. Y.; Yi, H. B.; Yuan, L.; Zhang, X. B. Enhancing the Anti-Solvatochromic Two-Photon Fluorescence for Cirrhosis Imaging by Forming a Hydrogen-Bond Network. *Angew. Chem. Int. Ed.* **2018**, *57*, 7473-7477.
26. Chen, W.; Pacheco, A.; Takano, Y.; Day, J. J.; Hanaoka, K.; Xian, M. A Single Fluorescent Probe to Visualize Hydrogen Sulfide and Hydrogen Polysulfides with Different Fluorescence Signals. *Angew. Chem. Int. Ed.* **2016**, *55*, 9993-9996.
27. Yin, J.; Kwon, Y.; Kim, D.; Lee, D.; Kim, G.; Hu, Y.; Ryu, J. H.; Yoon, J. Cyanine-Based Fluorescent Probe for Highly Selective Detection of Glutathione in Cell Cultures and Live Mouse Tissues. *J. Am. Chem. Soc.* **2014**, *136*, 5351-5358.
28. Gao, M.; Wang, R.; Yu, F.; You, J.; Chen, L. A Near-Infrared Fluorescent Probe for the Detection of Hydrogen Polysulfides Biosynthetic Pathways in Living Cells and in Vivo. *Analyst* **2015**, *140*, 3766-3772.
29. Sun, S. G.; Qiao, B.; Jiang, N.; Wang, J.; Zhang, S.; Peng, X. Naphthylamine-Rhodamine-Based Ratiometric Fluorescent Probe for the Determination of Pd²⁺ Ions. *Org. Lett.* **2014**, *16*, 1132-1135.
30. Wang, X.; Guo, Z.; Zhu, S.; Tian, H.; Zhu, W. A Naked-Eye and Ratiometric Near-Infrared Probe for Palladium via Modulation of a π -Conjugated System of Cyanines. *Chem. Commun.* **2014**, *50*, 13525-13528.
31. Pu, S. Z.; Ma, L. L.; Liu, G.; Ding, H. C.; Chen, B. A Multiple Switching Diarylethene with a Phenyl-Linked Rhodamine B Unit and Its Application as Chemosensor for Cu²⁺. *Dyes Pigm.* **2015**, *113*, 70-77.
32. Bae, S. K.; Heo, C. H.; Choi, D. J.; Sen, D.; Joe, E.; Cho, B. R.; Kim, H. M. A Ratiometric Two-Photon Fluorescent Probe Reveals Reduction in Mitochondrial H₂S Production in Parkinson's Disease Gene Knockout Astrocytes. *J. Am. Chem. Soc.* **2013**, *135*, 9915-9923.
33. Gao, M.; Wang, R.; Yu, F.; You, J.; Chen, L. Imaging and Evaluation of Sulfane Sulfur in Acute Brain Ischemia using a Mitochondria-Targeted Near-Infrared Fluorescent Probe. *J. Mater. Chem. B* **2018**, *6*, 2608-2619.
34. Gao, M.; Wang, R.; Yu, F.; You, J.; Chen, L. Evaluation of Sulfane Sulfur Bioeffects via a Mitochondria-Targeting Selenium-Containing Near-Infrared Fluorescent Probe. *Biomaterials* **2018**, *160*, 1-14.

35. Huang, Y.; Yu, F.; Wang, J.; Chen, L. Near-Infrared Fluorescence Probe for in Situ Detection of Superoxide Anion and Hydrogen Polysulfides in Mitochondrial Oxidative Stress. *Anal. Chem.* **2016**, *88*, 4122-4129.
36. Gao, M.; Yu, F.; Chen, H.; Che, L. Near-Infrared Fluorescent Probe for Imaging Mitochondrial Hydrogen Polysulfides in Living Cells and in Vivo. *Anal. Chem.* **2015**, *87*, 3631-3638.
37. Xuan, W.; Sheng, C. Q.; Cao, Y.; He, W.; Wang, W. Fluorescent Probes for the Detection of Hydrogen Sulfide in Biological Systems. *Angew. Chem. Int. Ed.* **2012**, *51*, 2282-2284.
38. Das, S. K.; Lim, C. S.; Yang, S. Y.; Han, J. H.; Cho, B. R. A Small Molecule Two-Photon Probe for Hydrogen Sulfide in Live Tissues. *Chem. Commun.* **2012**, *48*, 8395-8397.
39. Liu, C.; Peng, B.; Li, S.; Park, C.; Whorton, A. R.; Xian, M. Reaction Based Fluorescent Probes for Hydrogen Sulfide. *Org. Lett.* **2012**, *14*, 2184-2187.
40. Chen, S.; Chen, Z.; Ren, W.; Ai, H. Reaction-Based Genetically Encoded Fluorescent Hydrogen Sulfide Sensors. *J. Am. Chem. Soc.* **2012**, *134*, 9589-9592.
41. Peng, H. J.; Cheng, Y. F.; Dai, C. F.; King, A. L. B.; Predmore, L.; Lefer D. J.; Wang, B. A Fluorescent Probe for Fast and Quantitative Detection of Hydrogen Sulfide in Blood. *Angew. Chem. Int. Ed.* **2011**, *50*, 9672-9675.
42. Wang, R.; Yu, F.; Chen, L.; Chen, H.; Wang, L.; Zhang, W. A Highly Selective Turn-on Near-Infrared Fluorescent Probe for Hydrogen Sulfide Detection and Imaging in Living Cells. *Chem. Commun.* **2012**, *48*, 11757-11759.
43. Zhang, L.; Meng, W. Q.; Lu, L.; Xue, Y. S.; Li, C.; Zou, F.; Liu, Y.; Zhao, J. Selective Detection of Endogenous H₂S in Living Cells and the Mouse Hippocampus Using a Ratiometric Fluorescent Probe. *Sci. Rep.* **2014**, *4*, 5870.
44. Liu, Y.; Feng, G. A Visible Light Excitable Colorimetric and Fluorescent ESIPT Probe for Rapid and Selective Detection of Hydrogen Sulfide. *Org. Biomol. Chem.* **2014**, *12*, 438-445.
45. El Sayed, S.; de la Torre, C.; Santos-Figueroa, L. E.; Pérez-Payá, E.; Martínez-Mañez, R.; Sancenón, F.; Costero, A. M.; Parra, M.; Gil, S. A. A New Fluorescent "Turn-On" Chemodosimeter for the Detection of Hydrogen Sulfide in Water and Living Cells. *RSC Adv.* **2013**, *3*, 25690-25693.

46. Yang, X.; Wang, L.; Xu, H.; Zhao, M. A Fluorescein-Based Fluorogenic and Chromogenic Chemodosimeter for the Sensitive Detection of Sulfide Anion in Aqueous Solution. *Anal. Chim. Acta* **2009**, *631*, 91-95.
47. Fu, L.; Tian, F.; Lai, L.; Liu, Y.; Harvey, P. D.; Jiang, F. A Ratiometric "Two-In-One" Fluorescent Chemodosimeter for Fluoride and Hydrogen Sulfide. *Sensor Actuat B Chem.* **2014**, *193*, 701-707.
48. Liu, J.; Sun, Y.; Zhang, J.; Yang, T.; Cao, J.; Zhang, L.; Guo, W. A Ratiometric Fluorescent Probe for Biological Signaling Molecule H₂S: Fast Response and High Selectivity. *Chem. Eur. J.* **2013**, *19*, 4717-4722.
49. Liu, T. Y.; Zhang, X. F.; Qiao, Q. L.; Zou, C. Y.; Feng, L.; Cui, J. N.; Xu, Z. C. A Two-Photon Fluorescent Probe for Imaging Hydrogen Sulfide in Living Cells. *Dyes Pigm.* **2013**, *99*, 537-542.
50. Santos, F. S.; Ramasamy, E.; Ramamurthy, V.; Rodembusch, F. S. Excited State Behaviour of Benzoxazole Derivatives in a Confined Environment Afforded by a Water Soluble Octaacid Capsule. *J. Photochem. Photobiol. A Chem.* **2016**, *317*, 175-185.
51. Daengngern, R.; Kungwan, N. Dynamics Simulations of Photoinduced Proton Transfer Reactions of 2-(2'-Hydroxyphenyl)Benzoxazole in the Gas Phase and its Hydrated Clusters. *Chem. Phys. Lett.* **2014**, *609*, 147-154.
52. Padalkar, V. S.; Ramasami, P.; Sekar, N. A Comprehensive Spectroscopic and Computational Investigation of Intramolecular Proton Transfer in the Excited States of 2-(2'-Hydroxyphenyl)Benzoxazole and Its Derivatives. *J. Lumin.* **2014**, *146*, 527-538.
53. Douhal, A.; Amat-Guerri, F.; Lillo, M. P.; Acuña, A. U. Proton Transfer Spectroscopy of 2-(2'-Hydroxyphenyl)Imidazole and 2-(2'-Hydroxyphenyl)Benzimidazole Dyes. *J. Photochem. Photobiol. A Chem.* **1994**, *78*, 127-138.
54. Rodembusch, F. S.; Campo, L. F.; Leusin, F. P.; Stefani, V. Excited State Intramolecular Proton Transfer in Amino 2-(2'-Hydroxyphenyl)Benzazole Derivatives. Effects of the Solvent and the Amino Group Position. *J. Lumin.* **2007**, *126*, 728-734.
55. Lin, V. S.; Chen, W.; Xian, M.; Chang, C. J. Chemical Probes for Molecular Imaging and Detection of Hydrogen Sulfide and Reactive Sulfur Species in Biological Systems. *Chem. Soc. Rev.* **2015**, *44*, 4596-4618.
56. Lippert, A. R.; New, E. J.; Chang, C. J. Reaction-Based Fluorescent Probes for Selective Imaging of Hydrogen Sulfide in Living Cells. *J. Am. Chem. Soc.* **2011**, *133*, 10078-10080.

57. Zhang, J.; Guo, W. A New Fluorescent Probe for Gasotransmitter H₂S: High Sensitivity, Excellent Selectivity, and a Significant Fluorescence Off-On Response. *Chem. Commun.* **2014**, 50, 4214-4217.
58. Hou, P.; Chen, S.; Wang, H.; Wang, J.; Voitchovsky, K.; Song, X. An Aqueous Red Emitting Fluorescent Fluoride Sensing Probe Exhibiting a Large Stokes Shift and its Application in Cell Imaging. *Chem. Commun.* **2014**, 50, 320-322.
59. Oliveira, F. F. D.; Santos, D. C. B. D.; Lapis, A. A. M.; Corrêa, J. R.; Gomes, A. F.; Gozzo, F. C.; Moreira Jr., P. F.; de Oliveira, V. C.; Quina, F. H.; Neto, B. A. D. On the Use of 2,1,3-Benzothiadiazole Derivatives as Selective Live Cell Fluorescence Imaging Probes. *Bioorg. Med. Chem. Lett.* **2010**, 20, 6001-6007.
60. Qian, Y.; Karpus, J.; Kabil, O.; Zhang, S. Y.; Zhu, H. L.; Banerjee, R.; Zhao, J.; He, C. Selective Fluorescent Probes for Live-Cell Monitoring of Sulphide. *Nat. Commun.* **2011**, 2, Article number: 495.
61. Armarego, W. L. F. In: *Purification of Laboratory Chemicals*, 5th ed.; Elsevier Academic Press: Cornwall, UK, **2003**.
62. Wurth, C.; Grabolle, M.; Pauli, J.; Spieles, M.; Resch-Genger, U. Relative and Absolute Determination of Fluorescence Quantum Yields of Transparent Samples. *Nat. Protoc.* **2013**, 8, 1535-1550.
63. Eicher, T.; Hauptam, S.; Speicher, A. *The Chemistry of Heterocycles- Structure, Reactions, Syntheses and Application*, 2nd ed., Wiley-VCH GmbH, **2003**.
64. Vinodkumar, R.; Vaidya, S. D.; Kumar, B. V. S.; Bhise, U. N.; Bhirud, S. B.; Mashelkar, U. C. Synthesis, Anti-Bacterial, Anti-Asthmatic and Anti-Diabetic Activities of Novel *N*-Substituted 2-(4-Styrylphenyl)-1H-Benzimidazole and *N*-Substituted-3[4-(1H-Benzimidazole-2-yl)-Phenyl]-Acrylic Acid Tert-Butyl Ester. *Arkivoc* **2008**, 14, 37-49.
65. Yanai, T.; Tew, D. P.; Handy, N. C. A New Hybrid Exchange–Correlation Functional using the Coulomb-Attenuating Method (CAM-B3LYP). *Chem. Phys. Lett.* **2004**, 393, 51-57.
66. Gąsiorowski, P.; Matusiewicz, M.; Gondek, E.; Uchacz, T.; Wojtasik, K.; Danel, A.; Shchur, Ya.; Kityk, A. V. Synthesis and Spectral Properties of Methyl-Phenyl Pyrazoloquinoxaline Fluorescence Emitters: Experiment and DFT/TDDFT Calculations. *Opt. Mater.* **2018**, 75, 719-726.
67. Srivastava, R.; Al-Omary, F. A. M.; El-Emam, A. A.; Pathak, S. K.; Karabacak, M.; Narayan, V.; Chand, S.; Prasad, O.; Sinha, L. A Combined Experimental and Theoretical DFT (B3LYP, CAM-B3LYP And M06-2X) Study on Electronic Structure, Hydrogen

Bonding, Solvent Effects and Spectral Features of Methyl 1H-Indol-5-Carboxylate. *J. Mol. Struct.* **2017**, *1137*, 725-741.

68. Jang, H.; Kim, N. J.; Heo, J. Benchmarking Study on Time-Dependent Density Functional Theory Calculations of Electronic Circular Dichroism for Gas-Phase Molecules. *J. Comput. Theor. Chem.* **2018**, *1125*, 63-68.

69. Dunning, T. H. Gaussian Basis Sets For Use In Correlated Molecular Calculations. I. The Atoms Boron Through Neon And Hydrogen. *J. Chem. Phys.* **1989**, *90*, 1007-1023.

70. Papajak, E.; Zheng, J.; Xu, X.; Leverentz, H. R.; Truhlar, D. G. Perspectives on Basis Sets Beautiful: Seasonal Plantings of Diffuse Basis Functions. *J. Chem. Theory Comput.* **2011**, *7*, 3027-3034.

71. Tomasi, J.; Mennucci, B.; Cammi, R. Quantum Mechanical Continuum Solvation Models. *Chem. Rev.* **2005**, *105*, 2999-3094.

72. Martin, R. L. Natural transition orbitals. *J. Chem. Phys.* **2003**, *118*, 4775-4777.

73. Frisch, M. J.; Trucks, G. W.; Schlegel, H. B.; Scuseria, G. E.; Robb, M. A.; Cheeseman, J. R.; Scalmani, G.; Barone, V.; Petersson, G.A.; Nakatsuji, H.; Li, X.; Caricato, M.; Marenich, A. V.; Bloino, J.; Janesko, B. G.; Gomperts, R.; Mennucci, B.; Hratchian, H. P.; Ortiz, J.V.; Izmaylov, A. F.; Sonnenberg, J. L.; Williams-Young, D.; Ding, F.; Lipparini, F.; Egidi, F.; Goings, J.; Peng, B.; Petrone, A.; Henderson, T.; Ranasinghe, D.; Zakrzewski, V. G.; Gao, J.; Rega, N.; Zheng, G.; Liang, W.; Hada, M.; Ehara, M.; Toyota, K.; Fukuda, R.; Hasegawa, J.; Ishida, M.; Nakajima, T.; Honda, Y.; Kitao, O.; Nakai, H.; Vreven, T.; Throssell, K.; Montgomery, Jr., J. A.; Peralta, J. E.; Ogliaro, F.; Bearpark, M. J.; Heyd, J. J.; Brothers, E. N.; Kudin, K. N.; Staroverov, V. N.; Keith, T. A.; Kobayashi, R.; Normand, J.; Raghavachari, K.; Rendell, A. P.; Burant, J. C.; Iyengar, S. S.; Tomasi, J.; Cossi, M.; Millam, J. M.; Klene, M.; Adamo, C.; Cammi, R.; Ochterski, J. W.; Martin, R. L.; Morokuma, K.; Farkas, O.; Foresman, J. B.; Fox, D. J. Gaussian, revision A.03; Gaussian, Inc.: Wallingford, CT, **2016**.

74. Le Bahers, T.; Adamo, C.; Ciofine, I. A Qualitative Index of Spatial Extent in Charge-Transfer Excitations. *J. Chem. Theory Comput.* **2011**, *7*, 2498-2506.

75. Lu, T. Multiwfn, 2017 (08-May-2017) <https://www.multiwfn.codeplex.com>.

76. Andrienko, G. A. CHEMCRAFT, 2017 (08-May-2017) <http://www.chemcraftprog.com>